25
9-4-79
22 DYS

SAND79-0975
Unlimited Release

UC-11

Average Structure of the Upper Earth Mantle and Crust Between Albuquerque and the Nevada Test Site

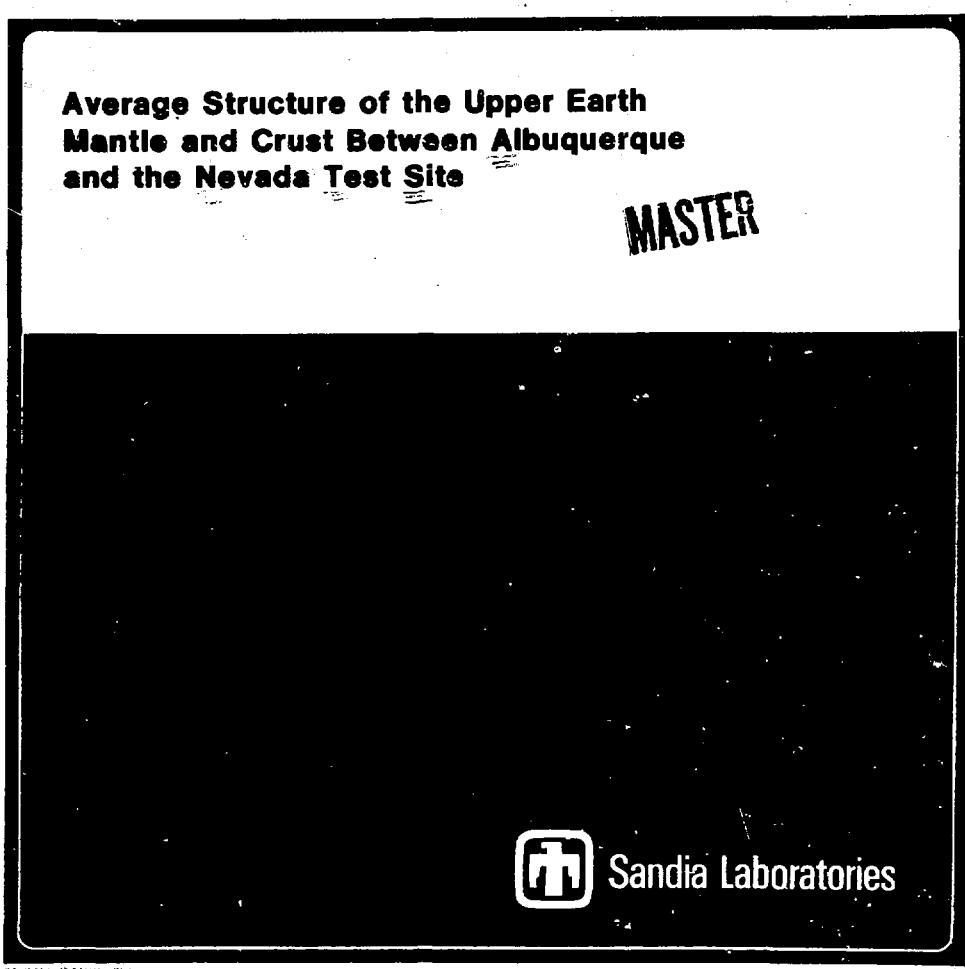

Sandia Laboratories

SAND79-0975
Unlimited Release
Printed August 1979

AVERAGE STRUCTURE OF THE UPPER EARTH MANTLE AND CRUST BETWEEN ALBUQUERQUE AND THE NEVADA TEST SITE

H. Douglas Garbin
Experiments Planning Division 1111
Sandia Laboratories
Albuquerque, NM 87185

ABSTRACT

We have constructed models of Earth structures by inverting seismic data obtained from nuclear events with a 1600-m-long laser strain meter. With these models we have been able to determine the general structure of the Earth's upper mantle and crust between Albuquerque and the Nevada Test Site.

CONTENTS

ILLUSTRATIONS

TABLES

AVERAGE STRUCTURE OF THE UPPER EARTH MANTLE AND CRUST BETWEEN ALBUQUERQUE AND THE NEVADA TEST SITE

Introduction

Inverting seismic data to construct models of earth structures is a common technique used in seismology. The knowledge obtained is of considerable interest to geophysicists for several reasons:

- The models derived can explain the composition of the Earth's crust and its tectonic evolution.
- Inferences of the chemical composition and physical state of the Earth's interior can be made.
- The Earth's transfer function can be studied with results that are of considerable value in determining seismic source mechanisms; this knowledge is useful in developing techniques to discriminate between natural and nuclear sources.

This paper investigates the possibility of inverting surface wave seismic data obtained from sources at the Nevada Test Site (NTS) by a single strain meter located in Albuquerque. The dispersion equation uses a modified Haskell method to incorporate earth sphericity effects.[1] This modified method has its greatest impact at larger wave periods (75 s). Corrections for gravity are not considered because the wave lengths are too short to be affected by gravity to any appreciable degree.

Many investigators have used long-range refraction lines and travel-time analyses to determine crust structure.[2-5] This is primarily a shallow structure method; however, deep body waves from teleseismic events have been used to estimate properties of the upper mantle. But, neither the shallow nor deep body wave methods will determine the shear wave velocity structure, so the investigator must invert the surface wave data to make such a determination.

Studies in surface wave inversion have been carried out for several years with data gathered over many different regions. Dorman and Ewing, McEvilly, Berry, and Knopoff, and Biswas and Knopoff are a few examples.[6-9] Recently, Bache, Rodi, and Harkrider determined the crust structure between NTS and Albuquerque with surface waves generated by NTS explosions.[10] This structure had been previously studied, using body waves[2-5] as well as surface waves.[9-11] All these studies provided useful background checks for our study on inversion.

The data for this study was obtained by a laser strain seismometer that Sandia Laboratories developed to monitor events at NTS. The design of the strain meter, which is located near Albuquerque, is similar to Jon Berger's 800-m-long strain meter at Piñon, CA, and its mode of operation is documented elsewhere.[12 13] The Sandia strain meter has a single 1600-m-long arm with its axis oriented toward NTS. Because relative displacement is measured with a Michelson interferometer, the instrument is extremely sensitive (5×10^{-11} strain), and has a flat response over the entire range of seismic frequencies.

The strain meter has been operational since 1975 and has recorded several nuclear events. Table 1 lists those events used in this study in addition to other information required for our analysis. Figure 1 is a map indicating the propagation path. Although this path runs southeasterly across a section of the Basin and Range Province, its major portion crosses the Colorado Plateau.

Table 1

Nuclear Events, NTS

Event	Δ (km)	m_b^*	M_s^{**}	Date	Shot Time
TYBO	932.79	5.7	4.4	5/13/75	1500:00:42
STILTON	939.96	5.6	4.4	6/03/75	1420:00:17
MAST	922.81	5.9	5.5	6/19/75	1300:00:09
KASSARI	929.11	6.2	5.9	10/28/75	1330:00:16
INLET	923.69	5.7	4.2	11/20/75	1400:00:09
CHIBERTA	894.88	5.5	5.0	12/20/75	1900:00:16
MUENSTER	921.59	6.0	6.1	1/03/76	1815:00:16
KEELSON	890.74	5.3	4.8	2/04/76	1320:00:11
ESROM	892.26	5.4	4.8	2/04/76	1340:00:16
FONTINA	935.27	6.2	5.9	2/12/76	1345:00:16
CHESHIRE	928.67	5.6	5.5	2/14/76	1030:00:16

* Body wave magnitude
** Surface wave magnitude

Since the nuclear events were physically close to each other, they had similar propagation paths and because the shot time was known, the phase velocities showed little scatter.

The estimates of wave magnitude were obtained from the Special Data Collection System Reports sponsored by the Defense Advanced Research Projects Agency (DARPA) and monitored by Vela, the multimedia program for monitoring nuclear bursts. The surface wave magnitude (M_s) ranges from 4.2 to 6.1. In the analysis, all the events contributed data for up to a wave period of about 40 s; however, for longer periods, only those events with larger surface wave magnitudes were used. At 75 s, only KASSARI, MUENSTER, and FONTINA produced usable data.

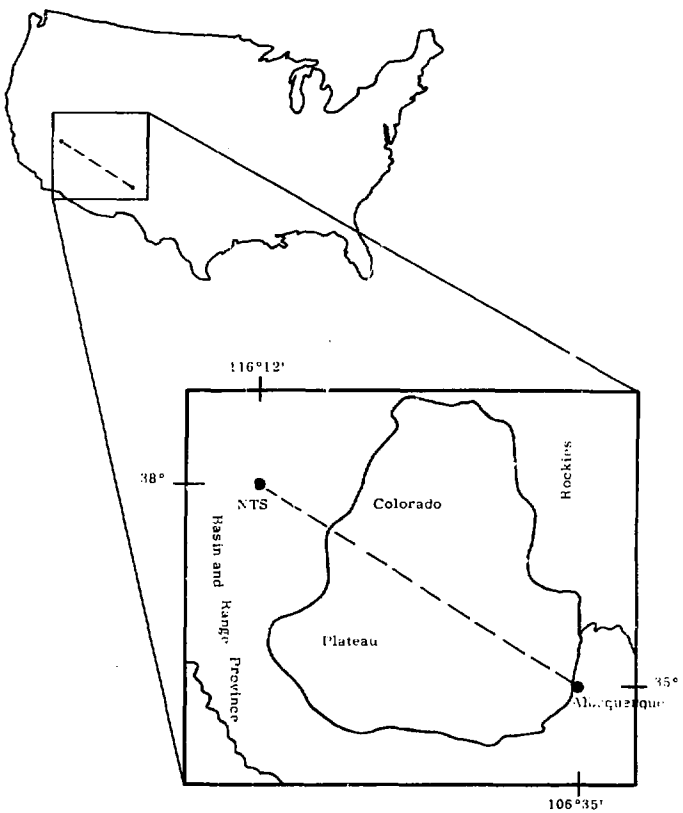

Figure 1. Propagation Path From NTS to Albuquerque

Phase Velocity Measurements

The literature describes several methods to determine phase velocity (c). In this study we used a single-station Fourier transform technique.[14 15] Briefly, if the horizontal displacement of the measured signal is given by f(t), then the Fourier transform of this signal is given as

$$F(\omega) = \int_0^\infty f(t)e^{-i\omega t}\, dt, \; f(t) = 0, \; t < 0 \; . \tag{1}$$

The spectrum is represented by the amplitude and phase functions

$$F(\omega) = |F(\omega)|\, e^{i\varphi} \; . \tag{2}$$

The phase term is $\varphi = \frac{5}{4}\pi + \theta_s - kr + \theta_i + 2\pi n$, $n = 0, 1, 2,$ etc... where θ_s is a time shift of the source phase, θ_i is an instrument phase shift, k is the wave number $(\frac{\omega}{c})$, and r is the range. In our case, $\theta_i = 0$. We added $2\pi n$ because the Fourier transform yields phase information only in the interval $(0, 2\pi)$. Therefore, by determining the phase spectrum from these data, the phase velocity is given by the following expression:

$$c = \frac{\omega r}{\theta_s(\omega) + \frac{5}{4}\pi - \varphi(\omega) + 2\pi n} \; . \tag{3}$$

The sources' phase shift can be estimated from theoretical considerations. There are several time source functions presented in the literature.[16 17 18] Haskell, and Mueller and Murphy have provided reasonably good representation because their models are based on close-in measurements of nuclear events; Haskell presents source measurements in terms of the reduced displacement potential. Archambeau relates this potential to the pressure response[19] at the elastic radius as described in Harkrider.[20] Mueller and Murphy represent this pressure response in an analytic form and estimate the parameters relating them to the close-in measurements. In either case, the phase shift is of the order $\frac{\pi}{2}$. Thus the equation used to determine the phase velocity is

$$c = \frac{\omega r}{-\varphi + \frac{1}{4}\pi + 2\pi n} \; . \tag{4}$$

We have added another $-\frac{\pi}{2}$ to Eq (3) because our data is obtained by a strain meter, yielding

$$\epsilon = \frac{\partial u_r}{\partial r} \approx -iku_r \; .$$

Treatment of the Data

We determined the value of φ from the data by first filtering over a narrow band and applying the Fast Fourier Transform (FFT) to the result in a window within which we expect the phase. With this method, we assume that the higher modes do not contribute significantly to the record. We based the estimates of the spectral contribution on Harkrider's calculations[21] and the higher modes may contribute about 2% of the amplitude in the period ranges of interest (5 to 75 s).

The method we used for inversion has been described by Dorman and Ewing, and Berry and Knopoff.[5,7] Although there are other methods, i.e., Bache et al[10] and Johnson and Gilbert,[22] linear inversion is more appropriate for our data. Briefly, we assume a spherical, layered structure in which the phase velocity is determined by a modified Haskell-Thomson function $F(c, p_i) = 0$. The p_i are the various geophysical parameters as

α_i - P wave velocity in ith layer
β_i - S wave velocity in ith layer
ρ_i - density in ith layer
d_i - thickness of ith layer.

A small increment, Δp_i, in parameters p_i, will produce a small increment in c_j, Δc_j, for a particular period T_j. This can be represented by the equation

$$\Delta c_j \frac{\partial F}{\partial c}(T_j) + \sum_i \frac{\partial F}{\partial p_i}(T_j)\,\Delta p_i = 0 \quad . \tag{5}$$

If there is more data than parameters, the redundancy is removed by a least-square fit of Eq (5). We then define S such that

$$S = \sum_j \left(\Delta c_j + \sum_i \frac{\frac{\partial F}{\partial p_i}}{\frac{\partial F}{\partial c}}\,\Delta p_i \right)^2 \quad . \tag{6}$$

The condition $\frac{\partial S}{\partial \Delta p_i} = 0$ results in a set of equations

$$\sum_j \Delta c_j \frac{\partial F}{\partial p_k} + \sum_j \sum_i \frac{\frac{\partial F}{\partial p_i}\frac{\partial F}{\partial p_k}}{\left(\frac{\partial F}{\partial c}\right)^2}\,\Delta p_i = 0 \quad . \tag{7}$$

$k = 1$, etc, N - parameters.

Previous studies on models have shown that Rayleigh wave velocities are determined primarily by S wave velocities, β_i, and layer thickness, d_i. Therefore, in this study, α_i and ρ_i will be constrained and values will be assumed from previous work on refraction and from Birch's relation[23] which is of the form

$$\alpha = -2.375 + 3.056\rho \tag{8}$$

when ρ is given in g/cm^3 and α in km/s.

By constraining some of the parameters, much of the nonuniqueness is removed. In addition, the insensitivity of α_i and ρ_i could produce unrealistic models. The following procedure requires that we assume a structure which is similar to the actual structure in which the phase velocities are calculated. With this structure, Δc_j is formed from the data and the model, and $\frac{\partial F}{\partial p_k}$ and $\frac{\partial F}{\partial c}$ are calculated by perturbing the structure and using the dispersion equation. The resultant inversion of Eq (7) yields Δp_k, and an iteration scheme is formed, which converges to a realistic model.

Earth Sphericity Corrections

The above discussion indicates that the ability to solve the inverse problem depends on calculating phase velocities and the partial derivatives $\frac{\partial F}{\partial p_i}$ and $\frac{\partial F}{\partial c}$. The Haskell-Thomson method yields solutions for plane, layered earth. Curvature and gravity effects can be introduced by an empirical formula suggested by Dorman and Ewing (Eq (9)).[5] Biswas and Knopoff[8] have also used this equation in their analysis and is given as

$$c_s = c_f (1 + 0.00016\ T) \tag{9}$$

where c_s is the phase velocity at period T (s) for a gravitating homogeneous sphere and c_f is the associating phase velocity for plane, layered earth without gravity.

For our analysis, this formula probably would have sufficed. Dorman and Ewing[5] claim that the formula is valid to ±1% for periods of 100 s < T < 300 s. Our largest period is 75 s.

However, with modifications to the Haskell-Thomson matrices, curvature effects can be incorporated into the technique without much effort. Hill first suggested a way to incorporate them and Bhattacharya made one extension.[24,25]

Our method is similar to Bhattacharya and differs mainly in how the physical parameters are viewed. Bhattacharya assumes that the velocities and densities in the sphere vary in such a way that he can reduce the spherical potential differential equations into the standard Cartesian

Helmholtz equations. This can be done if the layers are sufficiently thin. An alternative method --again, for sufficiently thin layers-- is based on the initial assumption that the velocities and densities in each spherical shell are constant. As indicated by Hill, if the P and SV components of the displacement equation decouple, then one can derive the spherical Helmholtz equations in terms of displacement potentials (ϕ, ψ). Applying the transformations to the Helmholtz equation

$$z = a \ln \frac{r}{a}$$

$$\phi_s = \left(\frac{a}{r}\right)^{\frac{1}{2}} \phi_f, \quad \psi_s = \left(\frac{a}{r}\right)^{\frac{1}{2}} \psi_f \tag{10}$$

where a is the earth's radius and r is the radial position, the following differential equation for the radial component may be obtained for the potentials ϕ_f and ψ_f:

$$\frac{d^2}{dz^2}\begin{pmatrix}\phi_f\\ \psi_f\end{pmatrix} + \left(\begin{pmatrix}k_\alpha^2\\ k_\beta^2\end{pmatrix} e^{-2z/a} - \frac{\ell(\ell+1)+\frac{1}{4}}{a^2}\right)\begin{pmatrix}\phi_f\\ \psi_f\end{pmatrix} = 0 \tag{11}$$

The potentials χ and ζ give the radial and SV components of displacement as defined in Eq (14). From Eq (11), we infer the following relations between flat and spherical media parameters:

$$\begin{aligned} \alpha_f &= \alpha_s e^{-z/a} = \alpha_s \frac{a}{r} \\ \beta_f &= \beta_s \frac{a}{r} \\ ka &= \ell - \frac{1}{2} \end{aligned} \tag{12}$$

where the subscript f and s refer to a flat and spherical structure, respectively. In order to apply the Haskell-Thomson method, the boundary conditions must also be transformed, using Eq (10). That is, the surface boundary conditions are

$$\begin{aligned} \tau_{rr} &= 0 \\ \tau_{r\theta} &= 0 \end{aligned} \tag{13}$$

and at each interface

$$\tau_{rr} = \tau_{rr}$$

$$\tau_{r\theta} = \tau_{r\theta}$$

$$u_r = u_r$$

$$u_\theta = u_\theta .$$

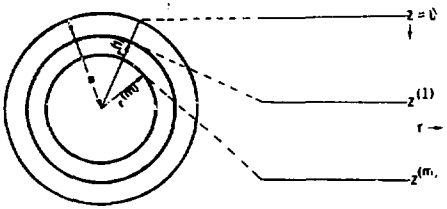

Figure 2. Transformation From Spherical to Flat Space

In the homogenous isotropic spherical shell, the displacement may be written as

$$\underline{u} = \nabla\phi + \nabla \times \nabla \times (\underline{r}\psi) \quad . \tag{14}$$

The SH portion of Eq (14) has already been decoupled out and neglected since we are interested in studying the Rayleigh wave. Both ϕ and ψ satisfy the spherical wave equation and when the transformations in Eq (10) are applied, they satisfy Eq (11). The components of stress and displacements (spherical earth) may be expressed as

$$u_r = \left[\frac{d\hat{\phi}}{dr} + \frac{\ell(\ell+1)}{r}\psi\right] P_\ell(\cos\theta) \tag{15}$$

$$u_\theta = -\frac{dP_\ell}{d\theta}\left[\frac{\phi}{r} + \frac{\xi}{r} + \frac{d\psi}{dr}\right]$$

$$\tau_{rr} = \left[-\lambda k_1^2\phi + 2\mu\frac{d^2\phi}{dr^2} - 2\mu\frac{\ell(\ell+1)}{r^2}\psi + 2\mu\frac{\ell(\ell+1)}{r}\frac{d\psi}{dr}\right] P_\ell$$

$$\tau_{r\theta} = 2\mu\frac{dP_\ell}{d\theta}\left[\frac{2}{r}\frac{d\phi}{dr} - \frac{2\hat{\phi}}{r^2} + \frac{d^2\psi}{dr^2} - \frac{2\psi}{r^2} + \frac{\ell(\ell+1)\psi}{r^2}\right] \quad .$$

Transforming the displacement and stresses into the z coordinate system (flat earth) gives

$$u_r = e^{-3z/2a}\left[-\frac{\phi_f}{2a} + \frac{d\phi_f}{dz} + \frac{\ell(\ell+1)}{a^2}\psi_f\right]$$

$$u_\theta = \frac{e}{a}^{-3z/2a}\left[\phi_f + \frac{\psi_f}{2a} + \frac{d\psi_f}{dz}\right] \tag{16}$$

$$\tau_{rr} = e^{-5z/2a}\left[2\mu\left[\frac{d^2\phi_f}{dz^2} + \frac{d^3\psi_f}{dz^3} + k_2^2\frac{d\psi_f}{dz}\right] - \lambda k_1^2\phi_f - \frac{4\mu}{a}\frac{d\phi_f}{dz}\right.$$

$$\left. + \frac{3\mu}{2a^2}\phi_f - \frac{3\mu}{a}\left(k^2 - \frac{1}{4a^2}\right)\psi_f - \frac{\mu}{4a^2}\frac{d\psi_f}{dz}\right]$$

$$\tau_{r\theta} = \frac{2\mu}{a}e^{-5z/2a}\left\{2\frac{d\phi_f}{dz} - \frac{3\phi_f}{a} + \left(\frac{2\ell(\ell+1)}{a^2} - k_2^2\right)\psi_f\right.$$

$$\left. - \frac{\psi_f}{a^2} - \frac{2}{a}\frac{d\psi_f}{dz}\right\} \quad .$$

Note that $ka = \ell + \frac{1}{2}$ or $\ell(\ell+1) = (ka)^2 - \frac{1}{4}$ and that the P_ℓ dependence has been dropped. By using the same notation in Harkrider[19] and assuming the same solution, i.e.,

$$\phi_m = \tilde{\Delta}'_m e^{-ikr\alpha_m z} + \tilde{\Delta}''_m e^{ikr\alpha_m z}$$

$$\psi_m = \tilde{\omega}'_m e^{-ikr\beta_m z} + \tilde{\omega}''_m e^{ikr\beta_m z} \quad , \qquad (17)$$

it can be shown that matrix, D_m, given by

$$D_m \begin{bmatrix} d_{11} & d_{12} & d_{13} & d_{14} \\ d_{21} & d_{22} & d_{23} & d_{24} \\ d_{31} & d_{32} & d_{33} & d_{34} \\ d_{41} & d_{42} & d_{43} & d_{44} \end{bmatrix} \tag{18}$$

where

$$d_{11} = -\left(\frac{\gamma_m}{c}\right)^2 \cos P_m$$

$$d_{12} = i\left(\frac{\alpha_m}{c}\right)^2 \sin P_m$$

$$d_{13} = \gamma_m\left(-r_{\beta_m} \cos Q_m - \frac{\sin Q_m}{2ka}\right)$$

$$d_{14} = i\gamma_m\left(r_{\beta_m} \sin Q_m - \frac{\cos Q_m}{2ka}\right)$$

$$d_{21} = i\left(\frac{\alpha_m}{c}\right)^2 \left(r_{\alpha_m} \sin P_m + \frac{\cos P_m}{2ka}\right)$$

$$d_{22} = -\left(\frac{\alpha_m}{c}\right)^2 \left(r_{\alpha_m} \cos P_m - \frac{\sin P_m}{2ka}\right)$$

$$d_{23} = i\gamma_m\left(-1 + \frac{1}{4(ka)^2}\right) \sin Q_m$$

$$d_{24} = \gamma_m\left(1 - \frac{1}{4(ka)^2}\right) \cos Q_m$$

$$d_{31} = -\rho_m \alpha_m^2 \left[\left(\gamma_m - 1 + \frac{3}{4}\frac{\gamma_m}{(ka)^2}\right) \cos P_m + 2\frac{\gamma_m r_{\alpha_m}}{ka} \sin P_m\right]$$

$$d_{32} = i\rho_m \alpha_m^2 \left[\left(\gamma_m - 1 + \frac{3\gamma_m}{4(ka)^2}\right) \sin P_m - \frac{2\gamma_m r_{\alpha_m}}{ka} \cos P_m\right]$$

$$d_{33} = -\rho_m c^2 \gamma_m^2 \left(1 - \frac{1}{4(ka)^2}\right)\left(r_{\beta_m} \cos Q_m - \frac{3 \sin Q_m}{2ka}\right)$$

$$d_{34} = \rho_m c^2 \gamma_m^2 \left(1 - \frac{1}{4(ka)^2}\right) \times \left(r_{\beta_m} \sin Q_m + \frac{3 \cos Q_m}{2ka}\right)$$

$$d_{41} = -i\rho_m \alpha_m^2 \gamma_m \left(r_{\alpha_m} \sin P_m + \frac{3}{2ka} \cos P_m\right)$$

$$d_{42} = \rho_m \alpha_m^2 \gamma_m \left(r_{\alpha_m} \cos P_m - \frac{3}{2ka} \sin P_m\right)$$

$$d_{43} = \rho_m c^2 \gamma_m i\left[\left(\gamma_m - 1 - \frac{3\gamma_m}{4(ka)^2}\right) \sin Q_m - \frac{\gamma_m r_{\beta_m}}{ka} \cos Q_m\right]$$

$$d_{44} = -\rho_m c^2 \gamma_m \left[\left[\gamma_m - 1 - \frac{3}{4}\frac{\gamma_m}{(ka)^2}\right] \times \cos Q_m - \frac{\gamma_m r_{\beta_m}}{ka} \sin Q_m\right].$$

relates the coefficients in the mth layer to the response at the boundary layer.

$$\left(\frac{\dot{U}_{in}}{c}, \frac{\dot{W}_m}{c}, \sigma_m, \tau_m\right) = D_m\left(\Delta'_m + \Delta''_m, \Delta'_m - \Delta''_m\ \omega'_m - \omega''_m, \omega'_m + \omega''_m\right) \tag{19}$$

Note that ka has been used in place of $\ell + \frac{1}{2}$. The notation is that used by Haskell and Harkrider:[1,20]

$$\begin{aligned} U_m &= \left(u_{\theta_m}\right) \\ W_m &= \left(u_{r_m}\right) \\ \sigma_m &= \left(\tau_{rr_m}\right) \\ \tau_m &= \left(\tau_{r\theta_m}\right) \end{aligned} \tag{20}$$

and

$$\begin{aligned} P_m &= kr_m d_m \\ Q_m &= kr_{\beta_m} d_m \\ d_m &= z_m - z_{m-1} \end{aligned} \tag{21}$$

Equation (19) is formed by putting $z = z_m$ in Eq (16) after using Eq (17). Also,

$$\begin{aligned} \tilde{\Delta}'_m &= -k^2\left(\frac{c}{\alpha_m}\right)^2 e^{-ikr_{\alpha_m} z_{m-1}}\ \tilde{\Delta}' \\ \tilde{\Delta}''_m &= -k^2\left(\frac{c}{\alpha_m}\right)^2 e^{ikr_{\alpha_m} z_{m-1}}\ \tilde{\Delta}'' \end{aligned} \tag{22}$$

$$\omega'_m = \frac{ik^3}{\gamma_m} e^{-ikr_{\beta_m} z_{m-1}}\ \tilde{\omega}'_m$$

and

$$\omega''_m = \frac{ik^3}{\gamma_m} e^{ikr_{\beta_m} z_{m-1}}\ \tilde{\omega}''_m \tag{23}$$

In a similar manner at $z = z_{m-1}$, it can be shown

$$\left(\frac{\dot{U}_{m-1}}{c}, \frac{\dot{W}_{m-1}}{c}, \sigma_{m-1}, \tau_{m-1}\right) = E_m\left(\Delta'_m + \Delta''_m, \Delta'_m - \Delta''_m, \omega'_m - \omega''_m, \omega'_m + \omega''_m\right) \tag{24}$$

where the continuity boundary conditions in Eq (13) have been used and E_m is given as

$$E_m = \begin{bmatrix} -\frac{\alpha_m^2}{c^2} & 0 & -\gamma_m r_{\beta_m} & -\gamma_m i/2ka \\ \frac{\alpha_m^2}{c^2}\frac{1}{2ka} & -\frac{\alpha_m^2}{c^2} r_{\alpha_m} & 0 & \gamma_m\left(1-\frac{1}{4(ka)^2}\right) \\ \rho_m\alpha_m^2\left(\gamma_m - 1 + \frac{3}{4}\frac{\gamma_m}{(ka)^2}\right) & -\frac{2i\rho_m\alpha_m^2\gamma_m r_{\alpha_m}}{ka} & -\rho_m c^2\gamma_m^2\left(1-\frac{1}{4(ka)^2}\right) r_{\beta_m} & \frac{3}{2}\frac{i\rho_m c^2\gamma_m^2}{ka}\left(1-\frac{1}{4(ka)^2}\right) \\ -\frac{i\rho_m\gamma_m\alpha_m^2}{2ka} & \rho_m\alpha_m^2\gamma_m r_{\alpha_m} & -\frac{i\rho_m\gamma_m^3 r_{\beta_m} c^2}{ka} & -\rho_m c^2\gamma_m\left(\gamma_m - 1 - \frac{3}{4}\frac{\gamma_m}{(ka)^2}\right) \end{bmatrix} \tag{25}$$

Note that E_m is equal to D_m when $P_m = Q_m = 0$. According to Eqs (19) and (24), the solution at one boundary may be related to an adjacent boundary symbolically as

$$\left(\frac{\dot{U}_m}{c}, \frac{\dot{W}_m}{c}, \sigma_m, \tau_m\right) = D_m E_m^{-1}\left(\frac{\dot{U}_{m-1}}{c}, \frac{\dot{W}_{m-1}}{c}, \sigma_{m-1}, \tau_{m-1}\right) \tag{26}$$

where E_m^{-1} is the inverse matrix to E_m and is given as

$$E_m^{-1} = \begin{bmatrix} -2\left(\frac{\beta_m}{\alpha_m}\right)^2\left(1-\frac{1}{4(ka)^2}\right) & -4\left(\frac{\beta_m}{\alpha_m}\right)^2\frac{i}{ka} & \frac{1}{\rho_m\alpha_m^2} & 0 \\ -\frac{1}{2ka}\frac{c^2\gamma_m}{\alpha_m^2 r_{\alpha_m}}\left(1-\frac{1}{4(ka)^2}\right) & \frac{c^2}{\alpha_m^2 r_{\alpha_m}}\left(\gamma_m - 1 + \frac{3\gamma_m}{4(ka)^2}\right) & \frac{i}{2ka\rho_m\alpha_m^2 r_{\alpha_m}} & \frac{\left(1-\frac{1}{4(ka)^2}\right)}{\rho_m\alpha_m^2 r_{\alpha_m}} \\ \left(\gamma_m - 1 - \frac{3\gamma_m}{4(ka)^2}\right)\frac{1}{\gamma_m r_{\beta_m}} & +\frac{3i}{r_{\beta_m} 2ka} & -\frac{1}{\rho_m r_{\beta_m}\gamma_m c^2} & \frac{-i}{\rho_m c^2 r_{\beta_m}\gamma_m 2ka} \\ \frac{-i}{ka} & 1 & 0 & \frac{1}{\rho_m\gamma_m c^2} \end{bmatrix} \tag{27}$$

The Haskell-Thomson matrix method continues developing in its usual form with the modified matrices D_m and E_m^{-1}. Defining

$$A_m = D_m E_m^{-1}$$

and by repeated iteration of Eq (26), the constants for the half space may be related to the topmost layer in the form

$$\left(\Delta'_n + \Delta''_n,\ \Delta'_n - \Delta''_n,\ \omega'_n - \omega''_n,\ \omega'_n + \omega''_n\right) = E_n^{-1} A_{n-1} A_{n-2} \cdots A_1 \left(\frac{\dot{U}_o}{c},\ \frac{\dot{W}_o}{c},\ \sigma_o,\ \tau_o\right) . \tag{28}$$

The half space is denoted by the n and the free surface by o.

The free surface boundary conditions are

$$\sigma_o = \tau_o = 0 .$$

Due to the sign convention, this implies that $\Delta'_n = \omega'_n = 0$. This condition ensures that the amplitude of surface waves decreases with depth. Equation (28) simplifies to the following form:

$$\left(\Delta'_n,\ -\Delta''_n,\ -\omega''_n,\ \omega''_n\right) = J\left(\frac{\dot{U}_o}{c},\ \frac{\dot{W}_o}{c},\ 0,\ 0\right) \tag{29}$$

where $J = E_n^{-1} A_{n-1} \cdots A_1$.

Eliminating Δ'_n, ω''_n, $\frac{\dot{U}_o}{c}$, $\frac{\dot{W}_o}{c}$ from the four equations results in a phase velocity dispersion relation given by

$$\frac{\dot{U}_o}{\dot{W}_o} = \frac{(J_{12} + J_{22})}{J_{11} + J_{21}} = -\frac{(J_{32} + J_{42})}{J_{31} + J_{41}} . \tag{30}$$

Thus, the phase velocity calculations for a spherical earth may be calculated from the dispersion Eq (30) in the same manner as in the flat earth case. In fact, from the modified matrices D_m and E_m^{-1}, it can be seen that sphericity effects enter as perturbations of the order $(ka)^{-1}$, and $(ka)^{-3}$ and in the limit of $a \to \infty$, we recover the flat earth model.

Equation (30) was compared with spherical models in the literature and was found to be in good agreement. In order to solve the potential differential Eq (11), we assume that α_f and β_f are constant and that they are replaced by an average calculated for each particular layer given by

$$\alpha_m = \frac{\alpha_s^{(m)}{}_a}{d_m}\left(\frac{a}{r^{(m-1)}} - \frac{a}{r^{(m)}}\right) . \tag{31}$$

There is a similar expression for β_m. $r^{(m)}$ are bounding radii of the spherical shells. This is identical to Schwab and Knopoff's procedure.[26]

Results

The total usable Rayleigh wave signal spanned a period range of from 5 to 75 s. The inversion process was carried out piecewise in which the topmost layers were determined first from the shorter wavelengths. The upper layers were then constrained and the lower portions of the structure successively calculated from the longer periods. This was done primarily to stabilize the inversion process. A short wavelength (20 km) will be affected little by the structure at a depth of 100 km. As a rule of thumb, if an interface was at a depth of H, the wavelengths most affected range from about 0.5 to 2 H.

Table 2 presents the initial model. Table 3 lists the corrected parameters after they have been inverted. The asterisks identify the active parameters. The bottom layers are not as well determined as the upper layers because of errors in analyzing the long periods (low S/N) and because the spread of data when sensing the structure. The FFT determines the phase at constant frequency intervals (Δf); however, the wavelengths are not constant and increasingly spread apart, resulting in a denser population of data at higher frequencies. In addition, the longest wavelength (T = 75 s) is about 280 km. This would sense to a depth of only 140 km.

Table 2

Initial Structure

Layer	α_m (km/s)	β_m (km/s)	ρ_m (g/cm^3)	d_m (km)
1	3.0	1.70	2.30	2.0
2	6.21	3.67	2.80	24.0
3	6.80	3.90	3.00	15.0
4	7.85	4.30	3.36	40.0
5	7.72	4.20	3.36	50.0
6	8.06	4.43	3.41	-

Table 3

Final Inverted Structure

Layer	α_m (km/s)	β_m (km/s)	ρ_m (g/cm^3)	d_m (km)	RMS (km/s)†
1	3.0	1.7	2.30	2.0	
2	6.21	3.665*	2.80	23.6*	0.0031
3	6.80	3.699*	3.00	14.8*	0.0024
4	7.85	4.259*	3.36	35.8*	0.0020
5	7.72	4.031*	3.36	103.6*	0.0067
6	8.06	4.430*	3.41	-	

†Root-mean-square (RMS) error in c is shown for each inversion downwards (d_m, β_m, β_{m-1}).

Figure 3 compares the final predicted with the observed dispersion. This curve compares favorably with that of Bache et al[10] but when comparisons were made with the longer periods as calculated by Biswas and Knopoff for the western US,[9] the velocities appeared a little low. Bache et al acquired their data along the same propagation path that we did, and, therefore, it is not surprising that both their and our dispersion curves are similar. But Bache et al were interested in crust studies and their phase velocity curve terminates at a period of 30 s. This limitation precludes comparing our longer periods with theirs. The discrepancy when comparing our long periods with those of Biswas and Knopoff can be explained by the fact that they used a different path. Our dispersion curve does fall in a generalized rift zone category as described by Knopoff.[27]

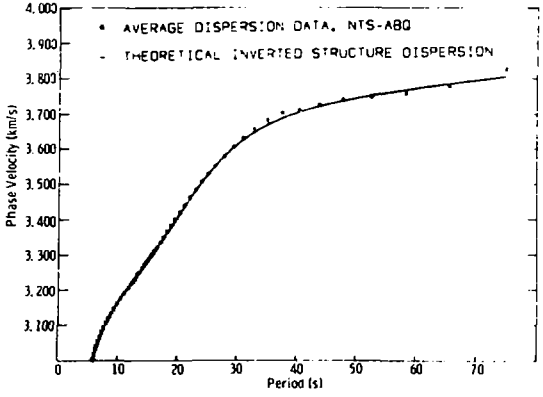

Figure 3. Predicted Dispersion Compared With Actual Dispersion

The crust layering also compares favorably to Bache who constraints the sediment and crust to depths of 2.5 km and 42 km, respectively. In our inversion, we constrained the sediment to a 2-km thickness and the crust was found at 40.4 km. However, as Bache points out, there is a great east-west variation in crust thickness and the above estimate is an average depth.

The shear velocities of the two models are also within reasonable limits. Bache's structure has much more detail in crust layers, whereas there are only two layers in our structure. Thus, his shear wave velocity varies from about 3.6 km/s at the top of the crust to 3.85 km/s near the Moho; his mantle velocity is about 4.25 km/s.

Our shear wave velocity in the crust is relatively constant at about 3.66 to 3.70 km/s and in the mantle, 4.26 km/s. The average crust velocity appears to be less than in the Bache structure, but it is not unreasonably so. Bache does not attempt to determine upper mantle properties since he treats the structure as a layered half space, the half space being the upper mantle.

Our study of long periods in the mantle produced low shear wave velocities compared with those of Biswas and Knopoff. The 4.1-km/s low velocity channel (LVC) in our study is very low and Biswas and Knopoff found no acceptable models that fitted in the neighborhood of our structure. Their models have velocities on the order of 0.3 to 0.8 km/s higher. This again is a result of having data only to a period of 75 s. However, even though I do not have much confidence in the actual LVC velocity, the data does seem to indicate the existence of such a layer.

We estimated error in our model by offsetting the phase velocities with a standard deviation of the data and by recalculating the model. Berry and Knopoff's method of using single parameter variations resulted in similar error estimates.[8] The consistency of the phase velocity calculation from the data of each of the 11 events was so good that it produced a root-mean-square (rms) error of about 0.007 km/s. The error analysis for the shorter periods estimated errors for β and h in this model of about ±0.01 km/s and ±1.0 km respectively.

Conclusions

Surface wave data from 11 events obtained by a laser strain seismometer were used to determine the average crust and upper mantle structure between NTS and Albuquerque. The phase velocities were determined by using an FFT over a window of the filtered seismogram and a phase velocity curve was determined by averaging over the 11 events. The linear inversion to determine the structure was done by using a modified Haskell-Thomson method with corrections for sphericity. The resulting models agreed with actual dispersion data, and had a standard error of only 0.007 km/s for the shorter period model and 0.027 km/s for the longer period model. The resulting structure agrees favorably with other studies at short periods, especially as represented by Bache. At the longer periods, there is less agreement, probably because of the different propagation paths used for other studies. Also, the nuclear events were not overly rich in low frequency energy and the signal was down considerably. Some longer period data is needed at these lower frequencies to obtain detailed results in the deeper layers.

References

[1] N. A. Haskell, "The Dispersion of Surface Wave on Multilayered Media," Seismolog Soc Am Bull, 43:17-43, 1953.

[2] C. B. Archambeau, E. A. Flinn, and D. G. Lambert, "Fine Structure of the Upper Mantle," J Geophysics Res, 74:5825-5865, 1969.

[3] R. C. Roller, "Crustal Structure in the Eastern Colorado Plateaus Province from Seismic-Refraction Measurements," Seismolog Soc Am Bull, 55:107-119, 1965.

[4] D. H. Warren, "A Seismic-Refraction Survey of Central Structure in Central Arizona," Geol Soc Bull 80:257-282, 1969.

[5] C. Prodehl, "Seismic Refraction Study of Crustal Structure in the Western United States," Geol Soc Bull 81:2629-2180, 1970.

[6] M. Ewing and J. Dorman, "Numerical Inversion of Seismic Surface Wave Dispersion Data or Crust-Mantle Structure in the New York-Pennsylvania Area," J Geophysics Res, 67:5227-5241, 1962.

[7] T. V. McEvilly, "Central U.S. Crust-Upper Mantle Structure from Love and Rayleigh Wave Phase Velocity Inversion," Seismolog Soc Am Bull 54:1997-2015, 1964.

[8] M. J. Berry and L. Knopoff, "Structure of the Upper Mantle Under the Western Mediterranean Basin," J Geophysics Res, 72:3613-3626, 1967.

[9] N. N. Biswas and L. Knopoff, "The Structure of the Upper Mantle Under the United States from the Dispersion of Rayleigh Waves," Geophys J R Astr Soc, 19:37-91, 1974.

[10] T. C. Bache, W. L. Rodi, and D. G. Harkrider, "Crustal Structures Inferred from Rayleigh-Wave Signatures of NTS Explosions," Seismolog Soc Am Bull, 68:1399-1413, 1978.

[11] G. R. Keller, R. B. Smith, R. Heaney, and D. H. Shurbert, "Upper Crustal Structure of the Eastern Basin and Range, Northern Colorado Plateau and Middle Rocky Mountains from Rayleigh-Wave Dispersion," Seismolog Soc Am Bull, 66:869-876, 1976.

[12] H. D. Garbin, Preliminary Analysis of Stream Seismic Response Recorded on Laser Strain Seismometer, SAND74-0123 (Albuquerque: Sandia Laboratories, September 1974).

[13] J. Berger and R. H. Lovberg, "Earth Strain Measurements with a Laser Interferometer," Science, 170:196-303, 1970.

[14] A. Ben-Menahem and M. N. Toksoz, "Source-Mechanism from Spectra of Long-Period Seismic Surface Waves, 3: The Alaska Earthquake of July 10, 1958," Seismolog Soc Am Bull, 53:905-920, 1963.

[15] A. M. Dziewonski and A. L. Hales, Methods in Computational Physics, 11 (New York: Academic Press, 1972), pp 46-49.

[16] N. A. Haskell, "Analytic Approximation for the Elastic Radiation from a Contained Underground Explosion," J Geophysics Res, 72:2583-2588, 1967.

[17] N. M. Toksoz, A. Ben-Menaham, and D. G. Harkrider, "Determination of Source Parameters of Explosions and Earthquakes by Amplitude Equalization of Seismic Surface Waves, 1: Underground Nuclear Explosions," J Geophysics Res, 69:4355-4366, 1964.

[18] R. A. Mueller and J. R. Murphy, "Seismic Characteristics of Underground Nuclear Detonations, Part I: Seismic Spectrum Scaling," Seismolog Soc Am Bull, 61:1675-1692, 1971.

[19]C. B. Archambeau, "The Theory of Stress Wave Radiation from Explosions in Prestressed Media," Geophysics J R Astr Soc, 29:329-366, 1972.

[20]D. G. Harkrider, "Surface Waves in Multilayered Elastic Media. I: Rayleigh and Love Waves from Buried Sources in a Multilayered Elastic Half-Space," Seismolog Soc Am Bull, 54:627-679, 1964.

[21]D. G. Harkrider, "Surface Waves in Multilayered Elastic Media. II: Higher Mode Spectra and Spectral Ratios from Point Sources in a Plane Layered Earth Models," Seismolog Soc Am Bull, 60:1937-1988, 1970.

[22]L. E. Johnson and F. Gilbert, Methods of Computational Physics, Vol 12 (New York: Academic Press, 1972), pp 231-266.

[23]F. Birch, "The Velocity of Compressional Waves in Rocks to 10 Kilobars, Part 2," J Geophysics Res, 66:2199-2224, 1961.

[24]D. P. Hill, An Earth-Flattening Transformation for Waves from a Point Source," Seismolog Soc Am Bull, 62:1195-1210, 1972.

[25]S. N. Bhattacharya, "Extension of the Thomson-Haskell Method to Non-Homogeneous Spherical Layers," Geophysics J R Astr Soc, 47:411-444, 1976.

[26]F. A. Schwab and L. Knopoff, Methods of Computational Physics, (New York: Academic Press, 1972, pp. 87-180.

[27]L. Knopoff, "Observation and Inversion of Surface-Wave Dispersion," Tectonophysics, 13:497-519, 1972.

DISTRIBUTION:

Los Alamos Scientific Laboratory
P. O. Box 1663
Los Alamos, NM 87545
Attn: K. H. Olsen, MS-676

Lawrence Livermore Laboratory (2)
P. O. Box 808
Livermore, CA 94550
Attn: K. K. Nakanishi, L-205
W. J. Hannon, L-205

US Department of Energy (3)
Division of Internal Security Affairs
20 Mass Ave.
Washington, DC 20545
Attn: R. T. Duff
R. H. Richards
J. L. Torres

Lt. Col. George V. Bulin, Jr.
Defense Advance Research Projects Agency
1400 Wilson Blvd
Arlington, VA 22209

Professor L. Knopoff
Institute of Geophysics and Planetary Physics
University of California, Los Angeles
Los Angeles, CA 90024

Professor E. Herrin
Geophysical Laboratory
Southern Methodist University
Dallas, TX 75275

Professor G. R. Keller
University of Texas, El Paso
Department of Geological Science
El Paso, TX 79968

Professor John Schlue
Department of Geosciences
New Mexico Tech University
Socorro, NM 8 301

T. C. Bache
Systems, Science, and Software
P. O. Box 1620
La Jolla, CA 92038

Professor Jon Berger
Institute of Geophysics and Planetary Physics
University of California, San Diego
La Jolla, CA 92093

1100 C. D. Broyles
1110 J. D. Kennedy
1111 J. R. Banister
1111 H. D. Garbin (4)
1111 G. E. Larsen
1111 S. D. Stearns
1111 L. J. Vortman
1112 C. R. Mehl
1120 T. L. Pace
1123 B. C. Benjamin
1125 H. C. Ogden
1130 H. E. Viney
1170 S. A. Moore
1253 A. C. Zuppero
1255 P. A. Stokes
Attn: D. R. Breding
H. B. Durham
8266 E. A. Aas
3141 T. L. Werner (5)
3151 W. L. Garner (3)
For DOE/TIC (Unlimited Release)
DOE/TIC (25)
(R. P. Campbell, 3154-3)